This stuff is installed. Installed does not mean there were not further edits after installation!

Appendix P: Eddy Currents and the Proximity Effect **1**
P.1 Eddy Current Analysis 1
P.2 Eddy currents in a thin round plate in a uniform B field 5
P.3 Eddy currents in a thin round plate in a *non*-uniform B field 8
(a) The stream function method in Cartesian Coordinates 9
(b) The stream function method in Cylindrical Coordinates 11
(c) Using the stream function method to solve the plate problem 12
P.4 Self-induced eddy currents in a round wire 16
P.5 Eddy currents induced in a quiet round-wire by an external B field 20
P.6 Eddy currents induced in an current-carrying wire by an external B field 23
P.7 Summary of Round Wire Examples 24
P.8 Eddy currents in Transmission Lines: The Proximity Effect 24
P.9 Quantitative Evaluation of Eddy Currents and The Proximity Effect 27
P.10 Influence of Proximity and Skin Effects on Wire Resistance 27

Appendix P: Eddy Currents and the Proximity Effect

P.1 Eddy Current Analysis

There are whole books on the subject of eddy currents, and the web reveals a plethora of papers and theses on eddy current applications. However, simple analytic examples of eddy current problems are hard to find. The general theory is quite complicated, and we present here a simplified approach which suits are limited purposes. We then work through some specific examples ending up with the implications of eddy currents for transmission lines.

Consider this drawing,

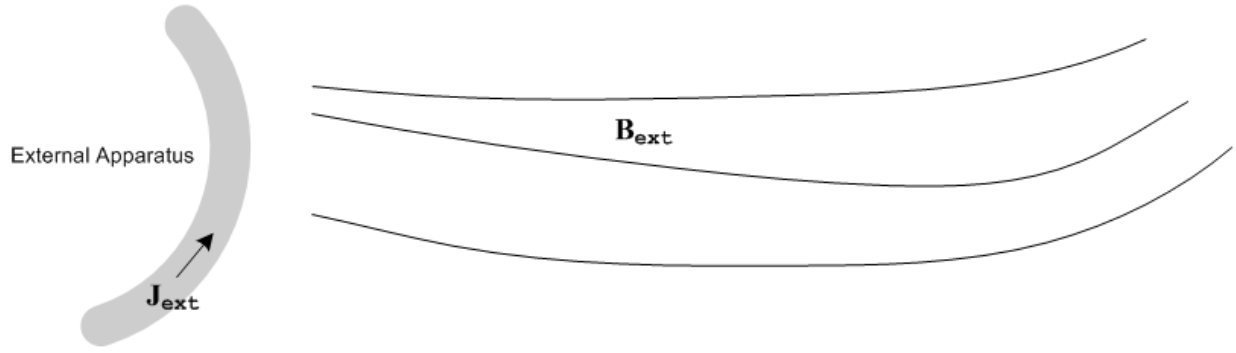

Fig P.1

An external apparatus has time-varying current density $\mathbf{J}_{ext}$ flowing in some wires and creates a time-varying magnetic field $\mathbf{B}_{ext}$.

We now bring in a **Device Under Test** (DUT) to obtain a new picture:

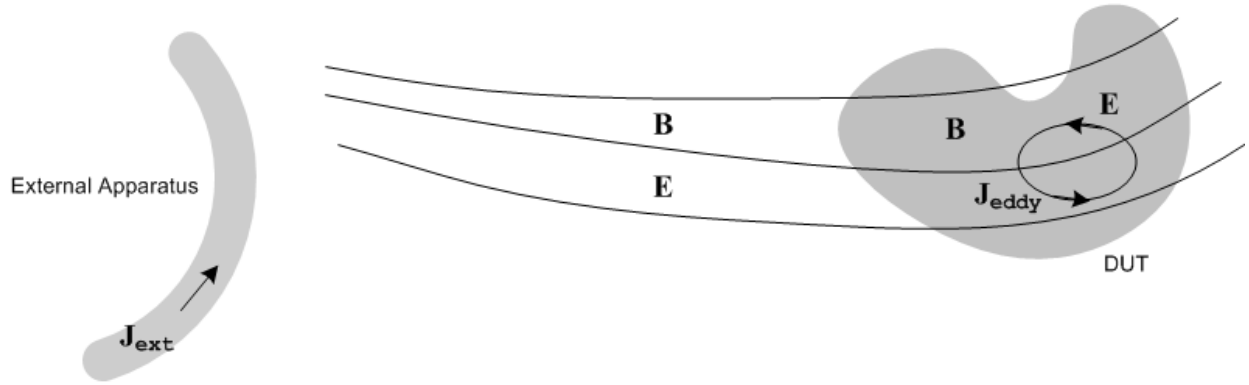

Fig P.2

For simplicity we assume that the DUT is non-magnetic ($\mu = \mu_0$) and is a good conductor with conductivity σ. We therefore ignore displacement currents inside the DUT, in accordance with the discussion below (2.2.2). Parameter ε applies to the region outside the DUT.

Iterative Interpretation

We now imagine the analysis of the **E** and **B** fields to take place in the following iterative sense, where we alternately consider the two Maxwell curl equations:

$\mathbf{E}^{(0)} = 0$	we assume no zeroth order electric field anywhere
curl $\mathbf{B_{ext}} = 0$	because $\mathbf{J_{ext}} = 0$ outside the external apparatus
curl $\mathbf{E}^{(1)} = -j\omega\mathbf{B_{ext}}$	time-changing $\mathbf{B_{ext}}$ creates $\mathbf{E}^{(1)}$ everywhere (Faraday)
$\mathbf{E} = \mathbf{E}^{(0)} + \mathbf{E}^{(1)} = \mathbf{E}^{(1)}$	which is superposed onto the existing $\mathbf{E}^{(0)} = 0$
$\mathbf{J_{eddy}}^{(1)} = \sigma\,\mathbf{E}^{(1)}$	$\mathbf{E}^{(1)}$ inside the DUT creates $\mathbf{J_{eddy}}^{(1)}$ in the DUT
curl $\mathbf{B_{eddy}}^{(1)} = \mu\mathbf{J_{eddy}}^{(1)}$	$\mathbf{J_{eddy}}^{(1)}$ in the DUT creates $\mathbf{B_{eddy}}^{(1)}$ in the DUT (Ampere)
curl $\mathbf{B_{eddy}}^{(1)} = j\omega\varepsilon\,\mathbf{E}^{(1)}$	and $\mathbf{B_{eddy}}^{(1)}$ also exists outside the DUT where $\mathbf{J_{eddy}} = 0$
$\mathbf{B} = \mathbf{B_{ext}} + \mathbf{B_{eddy}}^{(1)}$	This new $\mathbf{B_{eddy}}^{(1)}$ is superposed onto the original $\mathbf{B_{ext}}$
curl $\mathbf{E}^{(2)} = -j\omega\,\mathbf{B_{eddy}}^{(1)}$	$\mathbf{B_{eddy}}^{(1)}$ in turn results in a further adjustment to **E** (Faraday)
$\mathbf{E} = \mathbf{E}^{(1)} + \mathbf{E}^{(2)}$	which is then superposed onto the existing **E**
$\mathbf{J_{eddy}}^{(2)} = \sigma\mathbf{E}^{(2)}$	This new adjustment to **E** causes an adjustment in $\mathbf{J_{eddy}}$
curl $\mathbf{B_{eddy}}^{(2)} = \mu\mathbf{J_{eddy}}^{(2)}$	This in turn causes an adjustment to $\mathbf{B_{eddy}}$ in the DUT
curl $\mathbf{B_{eddy}}^{(2)} = j\omega\varepsilon\,\mathbf{E}^{(2)}$	and outside the DUT
$\mathbf{B_1} = \mathbf{B_{ext}} + \mathbf{B_{eddy}}^{(1)} + \mathbf{B_{eddy}}^{(2)}$	which is then superposed onto the existing B field.
curl $\mathbf{E}^{(3)} = -j\omega\mathbf{B_{eddy}}^{(2)})$	This in turn results in a new adjustment to **E**
$\mathbf{E} = \mathbf{E}^{(1)} + \mathbf{E}^{(2)} + \mathbf{E}^{(3)}$	which is then superposed onto the previous E field

and so on. (P.1.1)

Eventually we arrive at this situation inside the DUT

$$\text{curl}\,(\mathbf{E}^{(1)} + \mathbf{E}^{(2)} + ...) = -j\omega\,(\mathbf{B}_{\mathbf{ext}} + \mathbf{B}_{\mathbf{eddy}}{}^{(1)} + \mathbf{B}_{\mathbf{eddy}}{}^{(2)} + ...)$$

$$\begin{aligned}\text{curl}\,(\mathbf{B}_{\mathbf{ext}} + \mathbf{B}_{\mathbf{eddy}}{}^{(1)} + \mathbf{B}_{\mathbf{eddy}}{}^{(2)} + ...) &= \mu\sigma\,(\mathbf{E}^{(1)} + \mathbf{E}^{(2)} + ...) \\ &= \mu\,(\mathbf{J}_{\mathbf{eddy}}{}^{(1)} + \mathbf{J}_{\mathbf{eddy}}{}^{(2)} + ...)\end{aligned} \quad \text{(P.1.2)}$$

which, when all is said and done, is just an iterative interpretation of Maxwell's curl equations inside the DUT,

$$\begin{aligned}&\text{curl}\,\mathbf{E} = -j\omega\mathbf{B} \\ &\text{curl}\,\mathbf{B} = \mu\mathbf{J} = \mu(\sigma\mathbf{E})\end{aligned} \quad \text{(P.1.3)}$$

$$\begin{aligned}&\mathbf{B} = \mathbf{B}_{\mathbf{ext}} + \mathbf{B}_{\mathbf{eddy}}{}^{(1)} + \mathbf{B}_{\mathbf{eddy}}{}^{(2)} + ... \\ &\mathbf{E} = \mathbf{E}^{(1)} + \mathbf{E}^{(2)} + ... \\ &\mathbf{J} = \mathbf{J}_{\mathbf{eddy}}{}^{(1)} + \mathbf{J}_{\mathbf{eddy}}{}^{(2)} + ...\end{aligned} \quad \text{(P.1.4)}$$

One hidden assumption above is that $\mathbf{J}_{\mathbf{ext}}$ is not affected by the eddy currents and their fields, and we imagine this is implemented by some kind of current source control in the external apparatus.

Writing the solution of Maxwell's equations iteratively of course does not resolve the inherent complexity of the problem. For example, in the step above where we imagine computing $\mathbf{B}_{\mathbf{eddy}}{}^{(1)}$, we have to compute $\mathbf{B}_{\mathbf{eddy}}{}^{(1)}$ inside the DUT using curl $\mathbf{B}_{\mathbf{eddy}}{}^{(1)} = \mu\mathbf{J}_{\mathbf{eddy}}{}^{(1)}$ and then we have to compute $\mathbf{B}_{\mathbf{eddy}}{}^{(1)}$ outside the DUT using curl $\mathbf{B}_{\mathbf{eddy}}{}^{(1)} = j\omega\varepsilon\,\mathbf{E}^{(1)}$, and then we have to match the values of $\mathbf{B}_{\mathbf{eddy}}{}^{(1)}$ on the DUT boundary. This is a full-blown boundary problem that requires much effort to solve for a general DUT and is further complicated if the DUT is made of magnetic material.

Small ω

Looking at the above series of iterative steps, it would appear that if ω is in some sense "small", the series shown above for **B**,**E** and **J** are highly convergent and can be well approximated by the first one or two terms. In this situation, we have in essence a perturbation theory solution where ω is the smallness parameter. For very low frequencies, the key steps in the above iterative sequence are these:

$$\begin{aligned}&\text{curl}\,\mathbf{E}^{(1)} = -j\omega\mathbf{B}_{\mathbf{ext}} \\ &\mathbf{J}_{\mathbf{eddy}}{}^{(1)} = \sigma\,\mathbf{E}^{(1)}\end{aligned} \quad \text{(P.1.5)}$$

which we combine to get

$$\text{curl}\,\mathbf{J}_{\mathbf{eddy}}{}^{(1)} = -j\omega\sigma\mathbf{B}_{\mathbf{ext}} \quad \text{(P.1.6)}$$

and this will be the basis for the quantitative calculations of our first two examples below. Since ω is small, $\mathbf{J}_{\mathbf{eddy}}{}^{(1)}$ is small. The next iterative step

$$\text{curl } \mathbf{B}_{\mathbf{eddy}}^{(1)} = \mu \mathbf{J}_{\mathbf{eddy}}^{(1)} \tag{P.1.7}$$

then results in a small $\mathbf{B}_{\mathbf{eddy}}^{(1)}$, and then

$$|\mathbf{B}_{\mathbf{eddy}}^{(1)}| \ << \ |\mathbf{B}_{\mathbf{ext}}| \quad . \tag{P.1.8}$$

Although we present no formal proof, it seems likely that our simple perturbative eddy current analysis can only be viable at a frequency low enough that the skin depth δ is large compared to the dimensions of the DUT.

Larger ω

If ω is not small, we can still write (P.1.3) as

$$\begin{aligned} &\text{curl } \mathbf{E} = -j\omega(\mathbf{B}_{\mathbf{ext}} + \mathbf{B}_{\mathbf{eddy}}) \\ &\text{curl } (\mathbf{B}_{\mathbf{ext}} + \mathbf{B}_{\mathbf{eddy}}) = \mu \mathbf{J}_{\mathbf{eddy}} = \mu\sigma\mathbf{E} \end{aligned} \tag{P.1.9}$$

but the perturbation series interpretations of $\mathbf{B}_{\mathbf{eddy}}$, $\mathbf{J}_{\mathbf{eddy}}$ and $\mathbf{E}$ are not meaningful since they (probably) don't converge. In this case, we have a single monolithic problem that must be solved all at once by some method other than our simple iterative eddy current analysis starting with (P.1.6). What happens at higher frequencies is this: the external field $\mathbf{B}_{\mathbf{ext}}$ still creates eddy currents in the DUT, but these currents in turn generate $\mathbf{B}_{\mathbf{eddy}}$ fields which are large enough that they significantly alter $\mathbf{B}_{\mathbf{ext}}$ within the DUT and one must then deal with $\mathbf{B} \equiv \mathbf{B}_{\mathbf{ext}} + \mathbf{B}_{\mathbf{eddy}}$ as the true field which is causing those eddy currents. In this case, one can combine the two Maxwell curl equations into a wave / Helmholtz equation as we have done in (1.2.2) and later in (1.5.27) and (1.5.32), and then one must solve that Helmholtz equation subject to appropriate boundary conditions, both inside and outside the DUT. In effect we did this for an isolated round wire in Chapter 2 and the solution there involved extremely complicated **E** and **B** fields (recall the Kelvin functions) exhibiting skin effect and a rapidly winding phase as shown in Figure 2.9.

Despite the difficulty of the solution for larger ω, we know there exists a solution, and we can make qualitative observations about that solution based on the results of our simple low-ω example solutions. We shall do this below to provide an eddy current interpretation of both the skin effect in a round wire, and the proximity effect in a transmission line.

ECT Application

In typical **Eddy Current Testing** (ECT) systems, the frequency used might range from 10Hz to 1500 Hz. The idea of an ECT system is to try to detect $\mathbf{B}_{\mathbf{eddy}}$ using a sensitive Hall Effect or SQUID device, and take note of the field pattern produced by a DUT which is "known good" (has no internal cracks in the metal). An internal crack in a bad DUT will alter $\mathbf{J}_{\mathbf{eddy}}$ in some way, which in turn causes an alteration in $\mathbf{B}_{\mathbf{eddy}}$ which can hopefully be detected. Due to the skin depth penetration issue, the useful depth of such non-destructive testing systems might be up to 15 mm (ballpark). Higher ω generates a larger signal, gives more accuracy on the defect size and location, but penetration depth is less, so there is always a tradeoff. Often scans at different ω values are optimal for different depths of the defect. ECT is a subject of much current interest and many papers have been and are being written.

P.2 Eddy currents in a thin round plate in a uniform B field

To reduce symbol clutter, in this section we use the following notation in relation to Section P.1 :

$$\mathbf{B} \equiv \mathbf{B}_{\mathtt{ext}} \qquad \mathbf{J} \equiv \mathbf{J}_{\mathtt{eddy}}{}^{(1)} \tag{P.2.1}$$

A thin round plate of radius a and thickness h lies centered in the z = 0 plane of a cylindrical coordinate system. This plate is the Device Under Test (DUT) for this problem. An unseen external apparatus creates a time-varying and spatially uniform magnetic field $\mathbf{B} = B\,\hat{\mathbf{z}}$ perpendicular to the plate. The problem is to compute the electric field **E** in the plate, and the corresponding eddy currents $\mathbf{J} = \sigma\mathbf{E}$. The region surrounding the plate is assumed non-conducting, perhaps it is air.

Faraday's Law and symmetry imply circular closed electric field lines in the plate. We are perhaps more used to magnetic field lines being closed since div **B** = 0, but here we have closed electric field lines since div **E** = 0 inside the plate (since there is no free charge inside the plate, see Section 3.1). We assume sufficiently low ω so skin depth $\delta >> h$ (recall $\delta \equiv \sqrt{2/(\omega\mu\sigma)}$) so the E field lines are uniform in the z direction of the plate thickness. This is the implication of the word "thin" in discussing a "thin plate". In this drawing, the plate is gray, and some of the circular closed E field lines are shown in red,

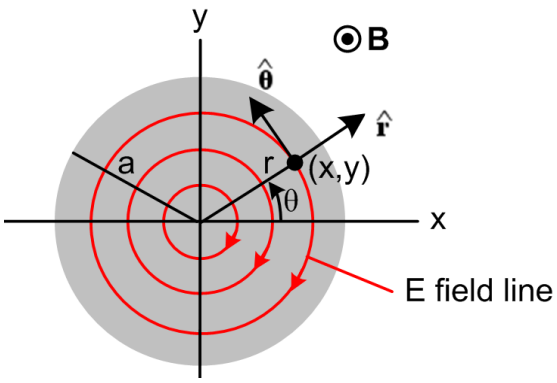

Fig P.3

The magnitude of the E field is constant on each circle due to symmetry. The field lines are drawn clockwise since we know by Lenz's Law that the associated eddy currents produce a B field opposed to the applied B field.

Since ω is small, we may use our first perturbation theory expansion term (P.1.6),

$$\text{curl}\ \mathbf{J}_{\mathtt{eddy}}{}^{(1)} = -j\omega\sigma\mathbf{B}_{\mathtt{ext}}\ . \tag{P.1.6}$$

Setting $\mathbf{J} \equiv \mathbf{J}_{\mathtt{eddy}}{}^{(1)}$, $\mathbf{B} \equiv \mathbf{B}_{\mathtt{ext}}$, $\mathbf{J} = \sigma\mathbf{E}$, and going into the time domain $j\omega \rightarrow \partial_t$ this says,

$$\text{curl}\ \mathbf{E} = -\,\partial_t\mathbf{B} \qquad \Leftrightarrow \qquad \oint_C \mathbf{E} \bullet d\mathbf{s} = -\partial_t\left[\int_S \mathbf{B} \bullet d\mathbf{S}\right]\ . \tag{P.2.2}$$

which we recognize as the Maxwell curl E equation and its integral form as shown in (1.1.36). Section P.1 has provided a context and an interpretation of the symbols **B**, **E** and $\mathbf{J} = \sigma\mathbf{E}$ appearing in (P.2.2).

Consider a circle at radius r. We then have from the right equation of (P.2.2),

$$E_\theta * 2\pi r = -\dot{B}\,\pi r^2 \quad \Rightarrow \quad E_\theta(r) = -\dot{B}\,\pi r^2/2\pi r = (-\dot{B}/2)\,r \ . \qquad \text{(P.2.3)}$$

The E field is linear in r, and is reminiscent of the result for the H field inside a round wire which carries a DC current I,

$$H * 2\pi r = I\,\pi r^2/\pi a^2 \quad =< \quad H(r) = I\,r^2/a^2 \,/\, 2\pi r = (I/2\pi a^2)r \ . \qquad \textit{(C.3.9)}$$

Notice that the E field line circles continue outside the plate and under and over it, but there will only be current in the plate. Here then is our result for **E** and **J** inside the plate:

$$\mathbf{E(r)} = E_\theta(r)\hat{\boldsymbol{\theta}} \qquad E_\theta(r) = (-\dot{B}/2)\,r \qquad J_\theta(r) = \sigma\,(-\dot{B}/2)\,r \ . \qquad \text{(P.2.4)}$$

We digress momentarily to study the heat loss generated in the plate. Consider a thin cylindrical shell of height dz and radius r and thickness dr. Think of this as a circular wire of rectangular cross section dA = dzdr. The current in this wire is given by,

$$dI = J_\theta\,dA = J_\theta\,dzdr \ . \qquad \text{(P.2.5)}$$

The resistance of the wire is $dR = \rho\,L/dA = \rho\,2\pi r/(dzdr)$ where $\rho = 1/\sigma$. The power burned from $P = I^2R$ is

$$dP = (dI)^2dR = [J_\theta\,dzdr]^2 * \rho\,2\pi r/(dzdr) = J_\theta^2\,[dzdr] * \rho\,2\pi r$$

$$= J_\theta^2\,2\pi r\rho\,dr\,dz = [\sigma\,(-\dot{B}_z/2)\,r]^2\,2\pi r\rho\,dr\,dz = (\pi/2)\sigma\,\dot{B}_z^2\,r^3\,drdz \ . \qquad \text{(P.2.6)}$$

Now integrate over the plate thickness h to replace dz by h. Then integrate r from 0 to a to get

$$P = (\pi/2)\sigma\,\dot{B}_z^2\,h(a^4/4) = (\pi/8)\sigma\,\dot{B}_z^2 a^4 h \ . \qquad \text{(P.2.7)}$$

Dimensions:
RHS = $[\text{ohm}^{-1}\text{m}^{-1}]\ \text{sec}^{-2}\ [\text{volt-sec/m}^2]^2\ \text{m}^5 = \text{ohm}^{-1}\text{sec}^{-2}\ [\text{volt-sec}]^2 = \text{volt}^2/\text{ohm} = \text{watts}$

The total current going around the plate as observed through any azimuthal slice $\theta = \theta_1$ is,

$$I = h\int_0^a dr\,J_\theta(r) = h\,\sigma\,(-\dot{B}_z/2)\int_0^a rdr = h\,\sigma\,(-\dot{B}_z/4)a^2 = -(1/4)\,h\sigma a^2\dot{B}_z \ . \qquad \text{(P.2.8)}$$

To summarize our conclusions for eddy currents in the thin round plate of radius a, thickness h and conductivity σ ,

$J_\theta(r) = -(1/2)\sigma\dot{B}\,r$ *(P.2.4)* // the eddy current density

$$I = -(1/4)\,\sigma h a^2 \dot{B} \qquad (P.2.8)$$

$$P = (\pi/8)\,\sigma h a^4 \dot{B}^2 \qquad (P.2.7) \qquad (P.2.9)$$

These results are in agreement with equations (36), (37) and (38) of Siakavellas. Since $\dot{B} \rightarrow j\omega B$, the power loss is proportional to the square of the frequency of the external B field, and it is proportional to the conductivity of the plate and its thickness. [Siakavellas also treats thin plates with polygonal boundaries.]

It is a simple matter now to plot the eddy current vector inside the plate:

$$J_x = J_\theta\ \hat{\theta}\bullet\hat{x} = -J_\theta \sin\theta = -J_\theta\,(y/r) = +(1/2)\,\dot{B}\sigma\, y \equiv ky\ \theta(r<a) \qquad k = (1/2)\,\dot{B}\sigma$$

$$J_y = J_\theta\ \hat{\theta}\bullet\hat{y} = J_\theta \cos\theta = J_\theta\,(x/r) = -(1/2)\,\dot{B}\sigma\, x \equiv -kx\ \theta(r<a)$$

With k = 1 and a = 1 Maple produces the following plot of the eddy currents inside the plate:

```
restart;with(plots):with(plottools):
k := 1:
a := 1:
Jx := k*y*Heaviside(a-r):
Jy := -k*x*Heaviside(a-r):
r := sqrt(x^2+y^2):
p1 := circle([0,0],a,color=red):
p2 := fieldplot([Jx,Jy], x=-a..a, y = -a..a, scaling=constrained, arrows=thick):
display(p1,p2);
```

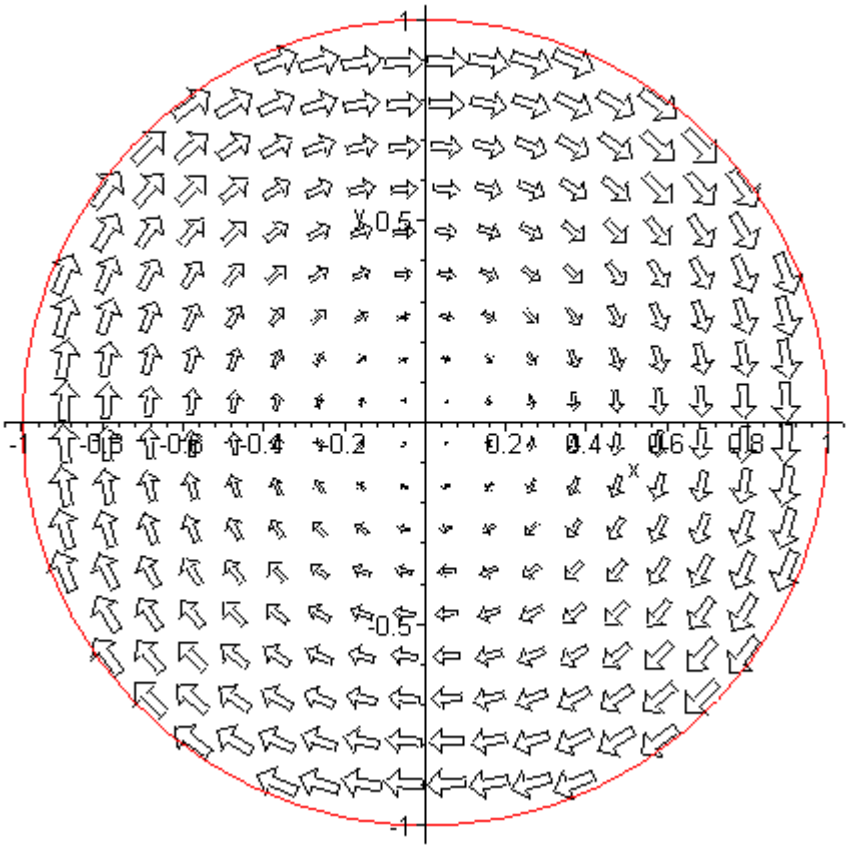

Fig P.4

With k = 1 we have assumed that $\dot{B} > 0$ (out of plane of paper), and according to Lenz's Law, the eddy current creates a B field whose flux cancels some of the applied B flux, hence the clockwise direction.

Reader Exercise. Notice that the $\mathbf{E}_{eddy}$ current arrows are largest near the edge of the plate according to (P.2.4) which says $E_\theta(r)$ = constant * r. Is it correct to interpret this as a 2D skin effect of the type encountered in Chapter 2? In terms of the external **B** field penetrating the disk, since the disk is thin we have assumed no skin effect in the z dimension and that **B** field penetrates fully and $\delta >> h$.

Reader Exercise. The EMF due to Faraday induction drives $\mathbf{J}_{eddy}$ in a tangential direction as Fig P.4 shows. Each conduction electron appears to maintain its radius from the disk center. Interpret this behavior in terms of the Lorentz force acting on the electron. Is there a "radial Hall effect" present in this problem? (see Appendix N)

P.3 Eddy currents in a thin round plate in a *non*-uniform B field

This example is the same as that of the previous section, *except* the B field is no longer spatially uniform and for simplicity we assume it has the following simple linear form,

$$B(x) = B_0 - \alpha x \qquad \alpha > 0 \qquad \text{// B(x) larger for x < 0 (on the left)} \qquad \text{(P.3.1)}$$

This is then a simple case where $\mathbf{B_{ext}}(\mathbf{x}) = \mathbf{B}(\mathbf{x})$ has a *gradient* over the plate.

Even with this simple form, the problem is considerably more complicated that the previous problem since we can no longer make use of azimuthal symmetry. First consider (P.2.2) now in the frequency domain, where as before $\mathbf{B} \equiv \mathbf{B_{ext}}$ and $\mathbf{E} = \mathbf{J_{eddy}}/\sigma$. (This equation is really (P.1.6) of Section P.1.)

$$\text{curl } \mathbf{E} = -\, j\omega \mathbf{B} \ . \qquad \textit{(P.2.2)} \qquad \text{(P.3.2)}$$

In cylindrical coordinates this says

$$\hat{\mathbf{r}}\,[\, r^{-1}\partial_\theta E_z - \partial_z E_\theta] + \hat{\boldsymbol{\theta}}\,[\partial_z E_r - \partial_r E_z] + \hat{\mathbf{z}}\,[\, r^{-1}\partial_r(rE_\theta) - r^{-1}\partial_\theta E_r\,] = -\, j\omega\, B\hat{\mathbf{z}} \quad . \qquad \text{(P.3.3)}$$

As in the previous example, we assume the plate is very thin and ω is very small so $\delta >> h$, so fields are constant in the z direction allowing us to replace $\partial_z \rightarrow 0$. At the same time, we assume $E_z = 0$ since E_z has no apparent source (and J_z has nowhere to flow). Then the above vector curl equation boils down to this scalar equation for the z component,

$$r^{-1}\partial_r(rE_\theta) - r^{-1}\partial_\theta E_r = -\, j\omega[B_0 - \alpha\, x]$$

or

$$\partial_r(rE_\theta) - \partial_\theta E_r = -\, j\omega[B_0 - \alpha\, r\cos\theta]r \qquad \text{(P.3.4)}$$

since $x = r\cos\theta$. Since there is no charge inside the plate (as before), we know div $\mathbf{E} = 0$, or

$$\text{div } \mathbf{E} = r^{-1}\partial_r(rE_r) + r^{-1}\partial_\theta E_\theta + \partial_z E_z = 0 \ . \qquad \text{(P.3.5)}$$

Again we set $E_z = 0$ (or $\partial_z \rightarrow 0$) which kills off the last term. Then (P.3.3) and (P.3.4) may be written

$$\partial_r(rE_\theta) - \partial_\theta E_r = -\, j\omega[B_0 - \alpha\, r\cos\theta]r$$

$$\partial_r(rE_r) + \partial_\theta E_\theta = 0 \quad . \qquad \text{(P.3.6)}$$

These equations form a system of coupled first-order linear PDE's in variables r and θ for functions $E_r(r,\theta)$ and $E_\theta(r,\theta)$. There is no z argument since we assumed $\partial_z \rightarrow 0$ above, so basically we have a 2D problem in polar coordinates. The first equation is inhomogeneous (has a driving term) while the second is homogeneous.

We wish to emphasize how the addition of a simple linear external B field variation has converted the trivial problem of Section P.2 to a non-trivial problem involving coupled partial differential equations. There are of course associated boundary conditions, such as $E_r(a,\theta) = 0$ since J_r can have no normal component at the rim of the plate. This complexity is typical of "eddy current problems". Below we shall solve this problem using a potential method, and one can then show that the solutions so obtained do in fact satisfy (P.3.6).

(a) The stream function method in Cartesian Coordinates

In our treatment of transmission lines in Chapter 4, we used the fact that div $\mathbf{B} = 0$ to describe the magnetic field in terms of a magnetic vector potential $\mathbf{A}$, where $\mathbf{B} = \text{curl } \mathbf{A}$ (since div curl $\mathbf{A} = 0$ for any

A). Under suitable conditions, it was then possible to ignore the "transverse" components of **A** and deal only with the z component A_z. This then replaced the complexity of three fields B_i with one field A_z.

In our current context of dealing with electric fields inside a conductor (where $\rho = 0$) we have div **E** = 0 and therefore div **J** = 0 since **J** = σ**E**. We can then describe the current **J** in terms of a *current* vector potential **T**, where **J** = curl **T** (since div curl **T** = 0 for any **T**). For a thin plate at low frequency ω, we will argue that the transverse components of **T** may be neglected, and then the complexity of three fields J_i is replaced by one field T_z, which is known in this context as a **stream function**.

Here then is the stream function method presented in Cartesian coordinates. First,

$$\mathbf{J} = \text{curl } \mathbf{T} = \hat{\mathbf{x}}\,(\partial_y T_z - \partial_z T_y) + \hat{\mathbf{y}}\,(\partial_z T_x - \partial_x T_z) + \hat{\mathbf{z}}\,(\partial_x T_y - \partial_y T_x)$$

$$\begin{aligned} J_x &= \partial_y T_z - \partial_z T_y \\ J_y &= \partial_z T_x - \partial_x T_z \\ J_z &= \partial_x T_y - \partial_y T_x \quad . \qquad \text{// components of the above} \end{aligned} \tag{P.3.7}$$

The **J** we have in mind is $\mathbf{J}_{eddy}^{(1)}$ appearing in (P.1.6). Using the symbols of (P.2.1), we have

$$\text{curl } \mathbf{J} = -j\omega\sigma\,\mathbf{B} \qquad \textit{(P.1.6)} \tag{P.3.8}$$

where $\mathbf{B} = B_z\,\hat{\mathbf{z}}$ [$= \mathbf{B}_{ext}$] . Using a standard vector identity we find then that

$$\text{curl } \mathbf{J} = \text{curl curl } \mathbf{T} = \text{grad}(\text{div } \mathbf{T}) - \nabla^2 \mathbf{T} \quad . \tag{P.3.9}$$

Just as we are allowed to work in the "Coulomb gauge" div **A** = 0 with the magnetic vector potential (see Appendix A), here we can work in the div **T** = 0 gauge for the current vector potential. In this gauge, we combine (P.3.8) and (P.3.9) to get

$$\nabla^2 \mathbf{T} = j\omega\sigma\mathbf{B} \tag{P.3.10}$$

where ∇^2 is the vector Laplacian operator. This equation can be compared with $\nabla^2\mathbf{A} = -\mu\mathbf{J}$ which is (1.3.5) for a magnetostatic situation where **A** has no time dependence. As shown in (H.1.9), equation (P.3.10) has the solution

$$\mathbf{T}(\mathbf{x}) = -\int d^3x'\,[1/4\pi R][j\omega\sigma\mathbf{B}] + \text{possible homogeneous solutions} \qquad R = |\mathbf{x}-\mathbf{x}'| \tag{P.3.11}$$

where the integral is the "particular solution" of (P.3.10). Since $\mathbf{B} = \mathbf{B}_{ext} = B_z(\mathbf{x})\,\hat{\mathbf{z}}$, the particular solution is entirely in the z direction. There may be some homogeneous adder solutions which create transverse components T_x and T_y, but we make the ansatz that

$$T_x, T_y << T_z \quad . \tag{P.3.12}$$

One motivation for this assumption is that then $J_z = \partial_x T_y - \partial_y T_x$ of (P.3.7) will be very small as we expect for a "thin" plate (we already assumed $E_z = 0$ above). Bypassing a detailed analysis of this issue, we shall assume that $T_x = T_y = 0$ and only T_z is significant. Then (P.3.7) becomes

$$\begin{aligned} J_x &= \partial_y T_z \\ J_y &= -\partial_x T_z \\ J_z &= 0 \quad . \end{aligned} \tag{P.3.13}$$

Furthermore, we assume that $T_z = T_z(x,y)$ with no z dependence, since then (P.3.13) will lead to currents J_x and J_y which have no z dependence. With all these assumptions, (P.3.10) becomes a scalar equation

$$\nabla_{2D}^2 T_z(x,y) = j\omega\sigma B_z(x,y) \tag{P.3.14}$$

where $\nabla_{2D}^2 \equiv \nabla^2 - \partial_z^2$ is the transverse component of the 3D scalar Laplacian.

Equation (P.3.14) is just the 2D Poisson equation of 2D potential theory [see (A.0.1) for the normal Poisson equation in 3D]. Many tools are available for solving this equation, and we shall use some of these tools below in our solution of the thin plate problem.

(b) The stream function method in Cylindrical Coordinates

In cylindrical coordinates (really polar coordinates) one writes

$$\nabla_{2D}^2 T_z = r^{-1}\partial_r(r\partial_r T_z) + r^{-2}\partial_\theta^2 T_z$$

so (P.3.14) becomes

$$r^{-1}\partial_r[r\partial_r T_z(r,\theta)] + r^{-2}\partial_\theta^2 T_z(r,\theta) = j\omega\sigma\, B_z(r,\theta) \quad . \tag{P.3.15}$$

The ansatz (P.3.12) becomes

$$T_r, T_\theta << T_z \quad . \tag{P.3.16}$$

The cylindrical replacement for (P.3.7) is

$$\mathbf{J} = \text{curl } \mathbf{T} = \hat{\mathbf{r}}\,[\, r^{-1}\partial_\theta T_z - \partial_z T_\theta] + \hat{\boldsymbol{\theta}}\,[\partial_z T_r - \partial_r T_z] + \hat{\mathbf{z}}\,[\, r^{-1}\partial_r(rT_\theta) - r^{-1}\partial_\theta T_r\,]$$

$$\begin{aligned} J_r &= r^{-1}\partial_\theta T_z - \partial_z T_\theta \\ J_\theta &= \partial_z T_r - \partial_r T_z \\ J_z &= r^{-1}\partial_r(rT_\theta) - r^{-1}\partial_\theta T_r \qquad \text{// components of the above} \end{aligned} \tag{P.3.17}$$

which, using (P.3.16), we approximate as

$$J_r = r^{-1}\partial_\theta T_z$$

$$J_\theta = -\partial_r T_z$$
$$J_z = 0 \qquad \text{(P.3.18)}$$

(c) Using the stream function method to solve the plate problem

From (P.3.1) we have $B_z(\mathbf{x}) = B_0 - \alpha\, x = B_0 - \alpha\, r\cos\theta$, so (P.3.15) states that

$$\partial_r[r\partial_r T_z(r,\theta)] + r^{-1}\partial_\theta^2 T_z(r,\theta) = j\omega\sigma\,[B_0 - \alpha\, r\cos\theta]\, r. \qquad \text{(P.3.19)}$$

Here we have a single second-order PDE in r,θ for a single function $T_z(r,\theta)$ [the stream function]. One can compare this with the pair of coupled first-order PDE's found earlier in (P.3.6).

Since the angle θ has the full range (0,2π) we can expand the various functions into "partial waves" as shown in (D.1.5) for a scalar function, so

$$T_z(r,\theta) = \sum_{m=-\infty}^{\infty} T_z(r,m)\, e^{jm\theta} \qquad \textit{(D.1.5a)}$$
$$T_z(r,m) = (1/2\pi) \int_{-\pi}^{\pi} d\theta\, T_z(r,\theta)\, e^{-jm\theta} \qquad \textit{(D.1.5b)} \qquad \text{(P.3.20)}$$

where we use our usual overloaded notation for T_z. Then (P.3.15) becomes, using $\partial_\theta \rightarrow +jm$,

$$\partial_r[r\partial_r T_z(r,m)] - r^{-1}m^2 T_z(r,m) = j\omega\sigma\, B_z(r,m)\, r \qquad \text{(P.3.21)}$$

where

$$B_z(r,m) = (1/2\pi) \int_{-\pi}^{\pi} d\theta\, B_z(r,\theta)\, e^{-jm\theta} = (1/2\pi) \int_{-\pi}^{\pi} d\theta\, [B_0 - \alpha\, r\cos\theta]\, e^{-jm\theta}$$

$$= B_0\,(1/2\pi) \int_{-\pi}^{\pi} d\theta\, e^{-jm\theta} - \alpha\, r\ (1/2\pi) \int_{-\pi}^{\pi} d\theta\, \cos\theta\, e^{-jm\theta}$$

$$= B_0\,(1/2\pi) \int_{-\pi}^{\pi} d\theta\, \cos(m\theta) - \alpha\, r\,(1/2\pi) \int_{-\pi}^{\pi} d\theta\, \cos\theta\, \cos(m\theta)$$

$$= B_0\ (1/\pi) \int_{0}^{\pi} d\theta\, \cos(m\theta) - \alpha\, r\ (1/\pi) \int_{0}^{\pi} d\theta\, \cos\theta\, \cos(m\theta)$$

$$= \delta_{m,0} B_0\ (1/\pi)\, \pi - \alpha\, r\ (1/\pi)\, \delta_{m,\pm 1}\, \pi/2$$

$$= \delta_{m,0} B_0 - (\alpha/2)\, r\, \delta_{m,\pm 1} \qquad \text{(P.3.22)}$$

where we use the following integral for integers m and n,

$$\int_0^{\pi} d\theta \cos(m\theta)\cos(n\theta) = \begin{cases} 0 & m \neq n \\ \pi/2 & m = n \neq 0 \\ \pi & m = n = 0 \end{cases} . \qquad \text{// Spiegel p 96 15.27}$$

Equations (P.3.21) become

$$\partial_r(r\partial_r T_z(r,0)) = j\omega\sigma B_0 r \qquad m = 0 \qquad \text{(P.3.23)}$$

$$\partial_r(r\partial_r T_z(r,\pm1)) - r^{-1}T_z(r,\pm1) = -j\omega\sigma(\alpha/2)r^2 \qquad m = \pm1 \qquad \text{(P.3.24)}$$

$$\partial_r(r\partial_r T_z(r,m)) - r^{-1}m^2 T_z(r,m) = 0 \qquad m = \text{other integers} \qquad \text{(P.3.25)}$$

We assume the solution to (P.3.25) is $T_z(r,m) = 0$. Maple tells us the general solutions to the first two equations,

```
restart: alias(I=I,j=sqrt(-1));
```

```
eq1 := diff(r*diff(Tz(r),r),r) = j*omega*sigma*B0*r;
```

$$eq1 := \left(\frac{\partial}{\partial r}Tz(r)\right) + r\left(\frac{\partial^2}{\partial r^2}Tz(r)\right) = j\,\omega\,\sigma\,B0\,r$$

```
dsolve(eq1);
```

$$Tz(r) = \frac{1}{4}j\,\omega\,\sigma\,B0\,r^2 + _C1 + _C2\ln(r)$$

```
eq2 := diff(r*diff(Tz(r),r),r)- (1/r)*Tz(r) = -(alpha/2)*j*omega*sigma*r^2;
```

$$eq2 := \left(\frac{\partial}{\partial r}Tz(r)\right) + r\left(\frac{\partial^2}{\partial r^2}Tz(r)\right) - \frac{Tz(r)}{r} = -\frac{1}{2}j\,\alpha\,\omega\,\sigma\,r^2$$

```
dsolve(eq2): simplify(%): expand(%);
```

$$Tz(r) = -\frac{1}{16}j\,\alpha\,\omega\,\sigma\,r^3 + r\,_C1 + \frac{_C1}{r} + r\,_C2 - \frac{_C2}{r}$$

We rename the constants to write these solutions as,

$$T_z(r,0) = j\omega\,\sigma\,B_0\,(1/4)r^2 + C_1\ln(r) + C_2$$

$$T_z(r,\pm1) = -(1/8)\,j\omega\sigma\,(\alpha/2)\,r^3 + D_1(r-1/r) + D_2(r+1/r) \; . \qquad \text{(P.3.26)}$$

To have $T_z(r,0)$ finite at $r = 0$ we must have $C_1 = 0$.
To have $T_z(r,\pm1)$ finite at $r = 0$ we must have $D_1 = D_2$. The solution forms are then

$$T_z(r,0) = j\omega\sigma\,B_0\,(1/4)\,r^2 + C_2$$
$$T_z(r,\pm1) = -(1/8)\,j\omega\sigma\,(\alpha/2)\,r^3 + 2D_1\,r \; . \qquad \text{(P.3.27)}$$

Inserting these partial wave amplitudes into (P.3.20) gives

$$T_z(r,\theta) = T_z(r,0) + T(r,+1)e^{j\theta} + T(r,-1)e^{-j\theta} = T_z(r,0) + T(r,+1)\,2\cos\theta$$

$$= [j\omega\sigma\, B_0\, (1/4)\, r^2 + C_2] + 2\cos\theta\, [-(1/8)\, j\omega\sigma\, (\alpha/2)\, r^3 + 2D_1\, r]$$

$$= [j\omega\sigma\, B_0\, (1/4)\, r^2 + C_2] - \cos\theta\, r\, [(1/8)\, j\omega\sigma\, \alpha\, r^2 - 4D_1] \ . \qquad \text{(P.3.28)}$$

At the origin point r = 0 we arbitrarily set the potential $T_z(0,\theta) = 0$ so $C_2 = 0$. One always has this freedom with a potential: since **J** = curl **T,** constants in **T** don't affect **J**. We then compute J_r as shown in (P.3.18) to obtain

$$J_r(r,\theta) = r^{-1}\partial_\theta T_z = \sin\theta\, [(1/8)\, j\omega\sigma\, \alpha\, r^2 - 4D_1] \ . \qquad \text{(P.3.29)}$$

But at r = a, we must have $J_r(a,\theta) = 0$ since there can be only tangential currents at the rim of our circular plate, and this determines D_1 giving this final result for the stream function T_z ,

$$T_z(r,\theta) = j\omega\sigma\, B_0\, (1/4)\, r^2 - (1/8)\cos\theta\, r\ j\omega\sigma\, \alpha\, (r^2 - a^2)$$

$$= j\omega\sigma\, [(1/4) B_0\, r^2 - (\alpha/8)\cos\theta\ (r^3 - a^2 r)] \ . \qquad \text{(P.3.30)}$$

The eddy current components are then, again from (P.3.18),

$$J_r(r,\theta) = r^{-1}\partial_\theta T_z = r^{-1}\, j\omega\sigma\, (\alpha/8)\sin\theta\, (r^3 - a^2 r) = j\omega\sigma\, [(\alpha/8)\sin\theta\, (r^2 - a^2)]$$

$$J_\theta(r,\theta) = -\partial_r T_z = j\omega\sigma\, [-(1/2) B_0\, r + (\alpha/8)\cos\theta\, (3r^2 - a^2)] \quad . \qquad \text{(P.3.31)}$$

Here then is a **summary** of the solution for a circular plate of radius r and conductivity σ in the presence of an external magnetic field $B(x) = B_0 - \alpha\, x$:

$$T_z(r,\theta) = j\omega\sigma\, [(1/4) B_0\, r^2 - (\alpha/8)\cos\theta\, r\ (r^2 - a^2)]$$

$$J_r(r,\theta) = j\omega\sigma\, [(\alpha/8)\sin\theta\, (r^2 - a^2)]$$
$$J_\theta(r,\theta) = j\omega\sigma\, [-(1/2) B_0\, r + (\alpha/8)\cos\theta\, (3r^2 - a^2)]$$

$$E_r(r,\theta) = j\omega\, [(\alpha/8)\sin\theta\, (r^2 - a^2)]$$
$$E_\theta(r,\theta) = j\omega\, [-(1/2) B_0\, r + (\alpha/8)\cos\theta\, (3r^2 - a^2)] \ . \qquad \text{(P.3.32)}$$

The eddy currents J_r and J_θ are proportional to ω as expected from (P.1.9a). Current J_r vanishes at the edge of the plate. When α = 0, we find $J_r(r,\theta) = 0$ and $J_\theta(r,\theta) = j\omega\sigma\, [-(1/2) B_0\, r]$ which replicates our uniform-B solution (P.2.4) which was $J_\theta(r) = \sigma\, (-\dot{B}/2)\, r$.

We have verified using Maple that the stream function $T_z(r,\theta)$ shown in (P.3.32) satisfies (P.3.19) and that the electric fields $E_r(r,\theta)$ and $E_\theta(r,\theta)$ satisfy (P.3.6).

Finally, we have Maple plot the resulting eddy currents. We first write

$$J_x = J_r\, \hat{\mathbf{r}} \bullet \hat{\mathbf{x}} + J_\theta\, \hat{\boldsymbol{\theta}} \bullet \hat{\mathbf{x}} = J_r \cos\theta - J_\theta \sin\theta$$

$$J_y = J_r\ \hat{r}\bullet\hat{y} + J_\theta\ \hat{\theta}\bullet\hat{y} \quad = J_r\ \sin\theta + J_\theta\ \cos\theta \quad . \tag{P.3.33}$$

For plotting we set $j\omega\sigma = 1$, $a = 1$, $B_0 = 1$, and $\alpha = 1$. Here is the plotting code,

```
Jr := (alpha/8)*(r^2-a^2)*sin(theta);
```

$$Jr := \frac{1}{8}\alpha\,(r^2 - a^2)\sin(\theta)$$

```
Jth := ( -B0*r/2 + (alpha/8)*cos(theta)*(3*r^2-a^2) );
```

$$Jth := -\frac{1}{2}B0\,r + \frac{1}{8}\alpha\cos(\theta)\,(3\,r^2 - a^2)$$

```
Jx := Jr*cos(theta)-Jth*sin(theta):
Jy := Jr*sin(theta)+Jth*cos(theta):
Jx1 := subs([sin(theta)=y/r,cos(theta)=x/r] ,Jx):
Jy1 := subs([sin(theta)=y/r,cos(theta)=x/r] ,Jy):
a := 1:  B0 := 1:alpha := 1:
r := sqrt(x^2+y^2):
Jx2 := Jx1*Heaviside(a-r):
Jy2 := Jy1*Heaviside(a-r):
p1 := circle([0,0],a,color=red):
p2 := fieldplot([Jx2,Jy2],
x=-a..a,y=-a..a,scaling=constrained,arrows=thick):
display(p1,p2);
```

and here is the resulting plot,

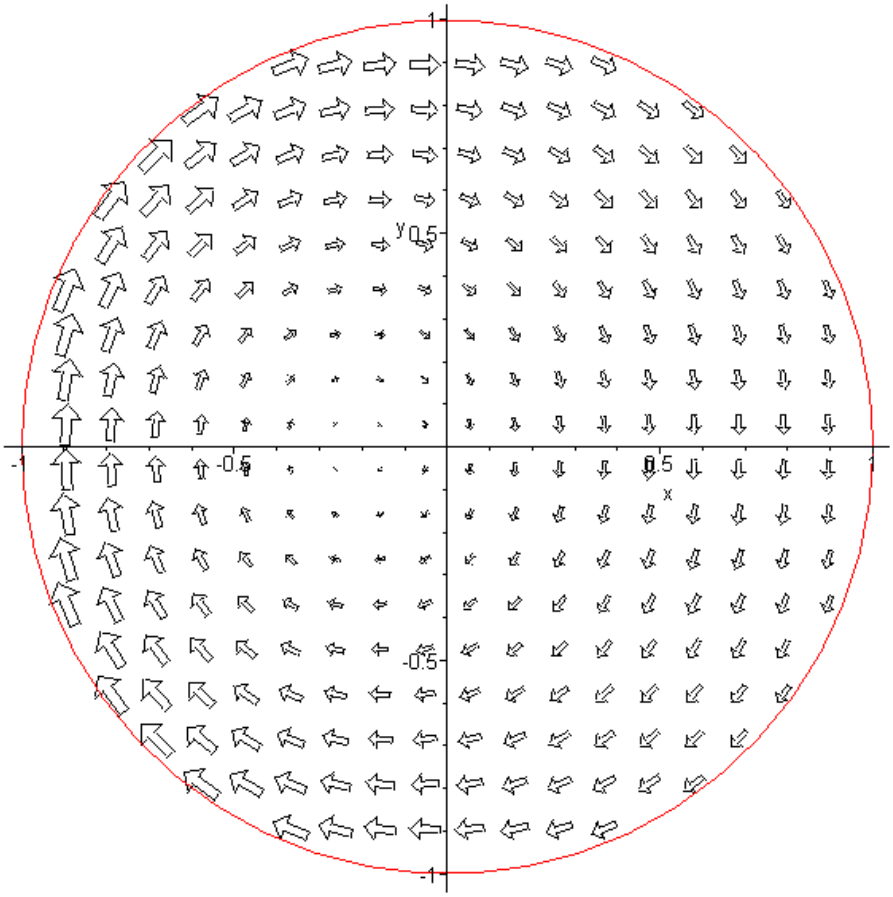

Fig P.5

which one can compare with the no-gradient plot of Fig P.4. As expected, the eddy currents are larger on the left side because the external B field is larger there. One can imagine the E field lines being a set of distorted circles which shrink down about a point to the left of the origin.

The main point of this example is to demonstrate the fact that a gradient in the external B field results in an *asymmetry* in the eddy current distribution such that the larger eddy current vectors are in the region in which the external B field is largest. We shall see below in a different geometry how this fact accounts for the so-called proximity effect in a transmission line.

P.4 Self-induced eddy currents in a round wire

We now reconsider our well-studied axially symmetric radius-a round wire of Chapter 2. In this eddy current example, the "external apparatus" and the "device under test" (DUT) are one in the same! In the zeroth order of the Section P.1 perturbation theory (very low ω), the current density in the wire is $\mathbf{J_{ext}}(\mathbf{x},\omega)$ which is perfectly uniform across the wire cross section and flows in the $\hat{\mathbf{z}}$ direction. This current density creates a magnetic field $\mathbf{B_{ext}}$ in the $\hat{\boldsymbol{\theta}}$ direction which is obtained from Ampere's Law,

$$2\pi r\, B_{ext}(r) = \frac{\pi r^2}{\pi a^2}\,\mu\, I_{enc} = \frac{\pi r^2}{\pi a^2}\,\mu\, J_{ext}\,\pi a^2 = \pi r^2 \mu J_{ext}$$

$$\Rightarrow\ B_{ext}(r) = (1/2)\,\mu\, r\, J_{ext}\,. \qquad \text{(P.4.1)}$$

In this problem the "external" current density $\mathbf{J_{ext}}$ is generated by the round wire itself, as if it were somehow its own "external apparatus". A better notation would be $\mathbf{J_{dc}}$ since this is the $\omega = 0$ current distribution, but we continue to use $\mathbf{J_{ext}}$ to maintain contact with the Section P.1. Similarly, $\mathbf{B_{ext}} = \mathbf{B_{dc}}$.

If the skin depth δ is large compared to the wire radius a, we expect the perturbation eddy current analysis of Section P.1 to be viable, and we write (P.1.6) as

$$\text{curl } \mathbf{J_{eddy}} \approx - j\omega\sigma \mathbf{B_{ext}} \qquad \text{where} \quad \mathbf{B_{ext}} = (1/2)\,\mu\, r\, J_{ext}\, \hat{\boldsymbol{\theta}} = B_{ext}(r)\, \hat{\boldsymbol{\theta}}. \tag{P.4.2}$$

In cylindrical coordinates one writes for an arbitrary vector field **F**,

$$\text{curl } \mathbf{F} = \hat{\mathbf{r}} \left[r^{-1}\partial_\theta F_z - \partial_z F_\theta \right] + \hat{\boldsymbol{\theta}} \left[\partial_z F_r - \partial_r F_z\right] + \hat{\mathbf{z}} \left[r^{-1}\partial_r(rF_\theta) - r^{-1}\partial_\theta F_r \right] . \tag{P.4.3}$$

For a vector field **F** which is a function only of r this reduces to,

$$\text{curl } \mathbf{F} = \hat{\boldsymbol{\theta}} \left[- \partial_r F_z\right] + \hat{\mathbf{z}} \left[r^{-1}\partial_r(rF_\theta) \right] . \tag{P.4.4}$$

Thus (P.4.2) becomes these two equations,

$$r^{-1}\partial_r[r(J_{eddy})_\theta] = 0$$

$$- \partial_r(J_{eddy})_z = -j\omega\sigma\, B_{ext}(r) = -j\omega\sigma\, (1/2)\,\mu\, r\, J_{ext} \quad . \tag{P.4.5}$$

The first equation of (P.4.5) may be written as

$$\partial_r[r(J_{eddy})_\theta] = 0$$

or

$$[r(J_{eddy})_\theta] = C_1$$

or

$$(J_{eddy})_\theta(r) = C_1/r$$

from which we must conclude that $C_1 = 0$ and then $(J_{eddy})_\theta(r) = 0$, so there is no azimuthal eddy current in the wire.

The second equation of (P.4.5) may be integrated from r=0 to r=r to obtain

$$(J_{eddy})_z(r) - (J_{eddy})_z(0) = j\omega\sigma\, (1/2)\,\mu\, J_{ext} \int_0^r dr'\, r' = j\omega\sigma\, (1/4)\,\mu\, J_{ext}\, r^2 . \tag{P.4.6}$$

Thus, the total current density in the wire obtained from eddy current analysis is in the z direction and is given by

$$J_z = J_{ext} + (J_{eddy})_z = J_{ext} + (J_{eddy})_z(0) + j\omega\sigma\, (1/4)\,\mu\, J_{ext}\, r^2$$

$$= J_{ext}\left[\,1 + \frac{(J_{eddy})_z(0)}{J_{ext}} \;+\; j\,\omega\mu\sigma\,(1/4)\,r^2\,\right]$$

$$\approx\; J_{ext}\left[\,1 \;+ j\,\omega\mu\sigma\,(1/4)\,r^2\,\right]. \qquad \text{// since } |(J_{eddy})_z(0)| \ll |J_{ext}| \text{ at low } \omega \tag{P.4.7}$$

Recall from (2.2.3) and (2.2.20) that

$$j\beta^2 = \omega\mu\sigma \;= 2/\delta^2 \;= |\beta^2| \qquad\qquad // \;\; j\omega\mu\sigma = -\beta^2 \tag{P.4.8}$$

where β is the complex Helmholtz parameter of (1.5.1). Therefore we have shown that

$$J_z = \; J_{ext}\left[\,1 \;+ j\,\omega\mu\sigma\,(1/4)\,r^2\,\right] = J_{ext}\left[\,1 - \beta^2(1/4)\,r^2\,\right]. \tag{P.4.9}$$

Notice that the eddy current contribution is $\pi/2$ out of phase with J_{ext}. Since we have assumed $\delta >> a$, it follows that

$$|\beta a| \;= (\sqrt{2}\,/\delta)\;a \;= \sqrt{2}\;\;(a/\delta) \;\ll 1 \tag{P.4.10}$$

so then $|\beta r| \ll 1$ and the eddy current contribution is very small, as required to use the first term in the perturbation expansion of Section P.1 as we have done. Defining

$$\kappa \;\equiv\; \omega\sigma\mu\,(1/4)r^2 \;=\; (j\beta^2)\,(1/4)\,r^2 \;=\; |\,\beta^2|\,(1/4)r^2 \;\ll 1$$
$$j\kappa \equiv j\omega\sigma\mu\,(1/4)r^2 \;= -\beta^2(1/4)\,r^2 \tag{P.4.11}$$

one finds

$$J_z = \; J_{ext}\left[\,1 - (\beta^2/4)r^2\right] \;= J_{ext}\left[\,1+j\kappa\,\right]$$
$$|J_z|^2 = |J_{ext}|^2\,(1+j\kappa)(1-j\kappa)$$
$$|J_z| = |\,J_{ext}\,|\;\sqrt{(1+j\kappa)(1-j\kappa)} \;= |\,J_{ext}\,|\;\sqrt{1+\kappa^2} \;\approx |\,J_{ext}\,|\;\left[\,1 + (1/2)\kappa^2\right] \tag{P.4.12}$$

so that

$$\frac{|J_z|}{|\,J_{ext}\,|} \;= \left[\,1 + (1/2)\kappa^2\right] \;= \left[\,1 + (1/2)\;\{\,|\,\beta^2|\,(1/4)r^2\,\}^2\right]$$
$$= \;1 + \frac{1}{2}\,\{(2/\delta^2)\,(1/4)r^2\}^2 \quad = \quad 1 + \frac{1}{2}\,\{(1/\delta^2)\,(1/2)r^2\}^2$$
$$= 1 + \frac{1}{8}\,(r/\delta)^4 \tag{P.4.13}$$

which then exhibits a very slight skin effect and has the same r dependence as (2.3.10), see Fig 2.7.

In Chapter 2 we found in (2.2.30) the following exact result for J_z in a round wire operating at ω,

$$J_z(r) = \frac{I}{2\pi a}\,\frac{J_0(\beta r)}{J_1(\beta a)}\,\beta \ . \qquad (2.2.30)$$

For small ω, since $|\beta r| << 1$, one has for small arguments [Spiegel 24.5 and 24.6]

$$J_0(x) \approx 1 - x^2/4$$

$$J_1(x) \approx (x/2)(1 - x^2/8) \quad \Rightarrow \quad 1/J_1(x) \approx (2/x)\,(1 + x^2/8) \ \approx \ (2/x) \qquad (P.4.14)$$

so

$$\frac{J_0(\beta r)}{J_1(\beta a)} \ \approx \ (2/\beta a)\,(1-\beta^2 r^2/4) \qquad (P.4.15)$$

and then

$$J_z(r) = \frac{I}{2\pi a}\ [(2/\beta a)\,(1-\beta^2 r^2/4)]\,\beta = \frac{I}{2\pi a}\ [(2/a)\,(1-\beta^2 r^2/4)] \ = \ \frac{I}{\pi a^2}\ [\,(1-\beta^2 r^2/4)]$$

$$= J_{ext}\ (1-\beta^2 r^2/4) \qquad (P.4.16)$$

in agreement with our eddy current analysis result (P.4.9).

At higher frequencies where we no longer have $\delta >> a$, the eddy current perturbation expansion diverges and becomes meaningless and one must instead solve the Helmholtz equation stated at the end of Section P.1. In Chapter 2 this task was in essence carried out and the skin effect was observed. One can then interpret the skin effect by saying that the eddy currents cancel the DC current density in the interior of the round wire, allowing a net current to exist only at the periphery. In other words, the skin effect is *caused* by eddy currents. But this is just a manner of speaking, and is like saying that the skin effect is "caused by Maxwell's Equations", which it is.

For a moderate skin effect, we can illustrate the eddy currents by crudely plotting them just in the central gray plane of the following drawing :

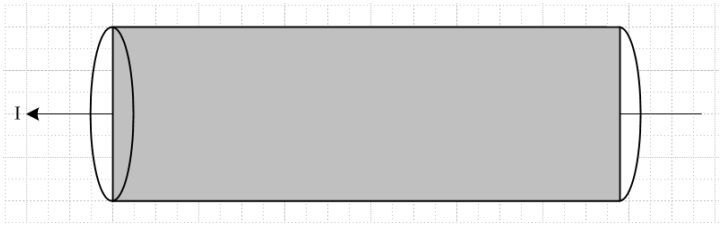

Fig P.6

Theses qualitative-only plots are for some particular instant in time. We know that the phase of J varies as shown in Fig 2.8, so we attempt to illustrate only the real parts the currents:

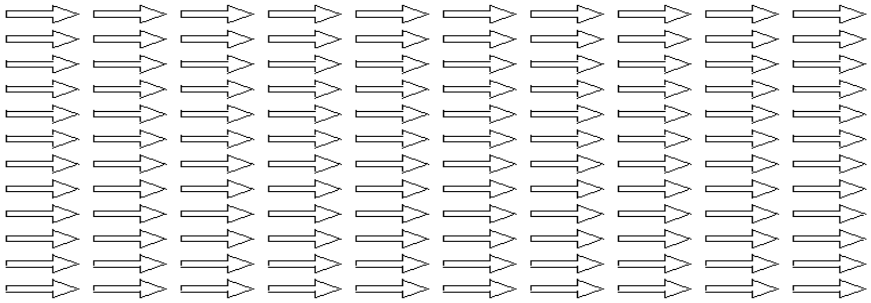

Re $\{J_{ext}\}$ Fig P.7 (a)

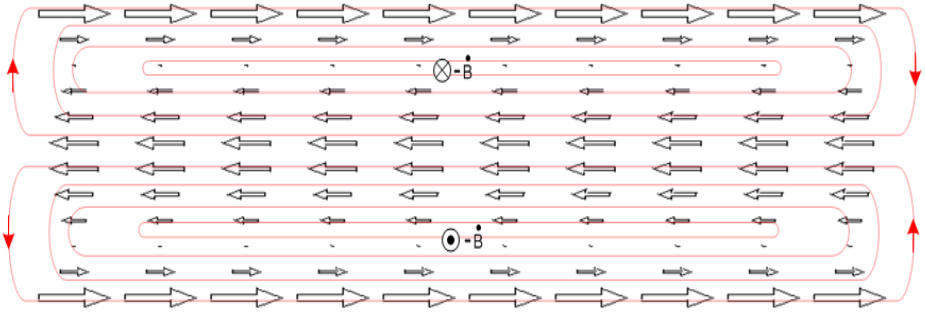

Re$\{J_{eddy}\}$ Fig P.7 (b)

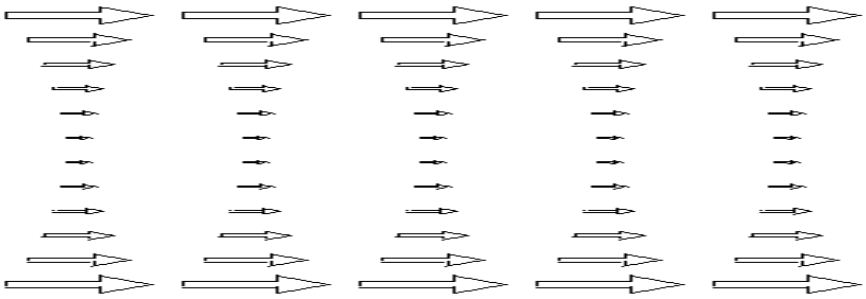

Re$\{J_{ext}+J_{eddy}\}$ Fig P.7 (c)

The closed red curves in Fig P.7 (b) represent the $\mathbf{J}_{eddy}$ field lines, and these then represent the actual induced "eddies" of current. One could write $\mathbf{J}_{eddy} = \sigma\, \mathbf{E}_{eddy}$ and then they are electric field lines. The lines close on themselves because they have no sources: inside the wire $\rho = 0$ so div $\mathbf{J}_{eddy} = 0$ and div $\mathbf{E}_{eddy} = 0$. Recall that a field in general does not have a constant magnitude along a field line. In the geometry of a round wire, the field lines in fact loop around at the ends of the wire.

P.5 Eddy currents induced in a quiet round-wire by an external B field

Uniform B_{ext}

In this example, we start with our Device Under Test (DUT) which is a straight round wire which carries no current. Some "external apparatus" creates a time-changing magnetic field $\mathbf{B}_{ext} = B_{ext}\hat{\mathbf{y}}$ as shown in

the figure below, where $\mathbf{B_{ext}}(\mathbf{x},\omega)$ is for the moment constant in space. At the instant in time shown, the time-domain field $\mathbf{B_{ext}}(\mathbf{x},t)$ is increasing in the $-\hat{\mathbf{y}}$ direction so that $-\dot{\mathbf{B}}_{\mathbf{ext}}(\mathbf{x},t)$ points in the $+\hat{\mathbf{y}}$ direction, out of the plane of paper.

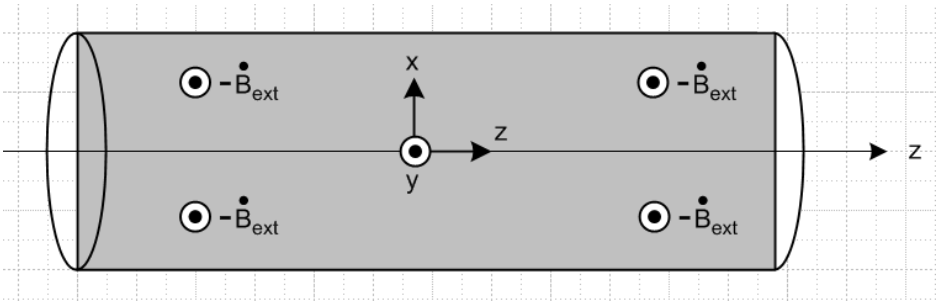

Fig P.8

The time-domain eddy current equation (P.1.6) (we assume small ω) and its integral form are

$$\text{curl } \mathbf{J_{eddy}} = \sigma\,[-\dot{\mathbf{B}}_{\mathbf{ext}}] \quad \Leftrightarrow \quad \oint_C \mathbf{J_{eddy}} \bullet d\mathbf{s} = \sigma \int_S [-\dot{\mathbf{B}}_{\mathbf{ext}}] \bullet d\mathbf{S} \quad . \tag{P.5.1}$$

The integral form implies that the flux change through any math loop in the gray rectangle is positive at our time instant, so according to the right hand rule, the eddy currents in the gray rectangle have the following general shape,

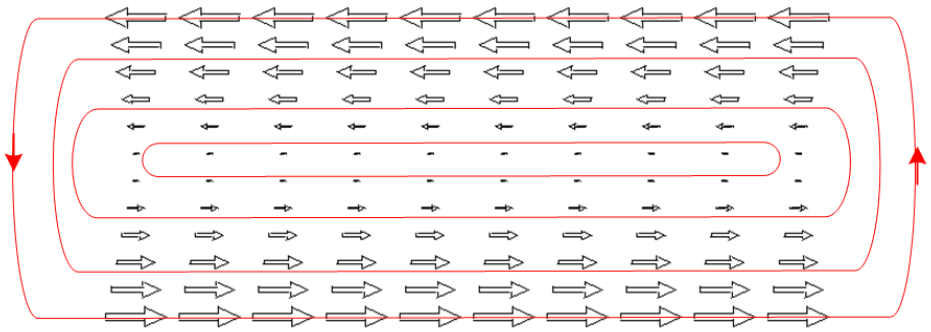

Fig P.9

This figure is analogous to Fig P.4 above which shows the eddy current in a thin round plate for a uniform external B field.

To justify the linear variation with x (vertical), if we assume that away from the ends of the wire nothing varies with z, and if we write $\mathbf{J_{eddy}}$ as $\mathbf{J}$, we find that

$$\text{curl } \mathbf{J} = \hat{\mathbf{x}}\,(\partial_y J_z - \partial_z J_y) + \hat{\mathbf{y}}\,(\partial_z J_x - \partial_x J_z) + \hat{\mathbf{z}}\,(\partial_x J_y - \partial_y J_x) = -\sigma\,\dot{\mathbf{B}}_{\mathbf{ext}}\hat{\mathbf{y}}$$

or

$$\hat{\mathbf{x}}\,(\partial_y J_z) + \hat{\mathbf{y}}\,(-\partial_x J_z) + \hat{\mathbf{z}}\,(\partial_x J_y - \partial_y J_x) = -\sigma\,\dot{\mathbf{B}}_{\mathbf{ext}}\hat{\mathbf{y}} \tag{P.5.2}$$

which produces the three equations

$$\partial_x J_z = \sigma \dot{B}_{ext} \qquad \Rightarrow J_z(x) = \sigma \dot{B}_{ext}\, x \quad // \text{ linear in x}$$

$$\partial_y J_z = 0 \qquad \Rightarrow J_z = J_z(x) \text{ only}$$

$$\partial_x J_y - \partial_y J_x = 0 \qquad \text{satisfied if } J_x \text{ and } J_y = 0 \qquad \text{(P.5.3)}$$

The eddy pattern in the round wire would have the same general appearance in any slice of the wire parallel to the slice shown as the gray rectangle in Fig P.8. The current of course drops to 0 at the wire surface since we assume the wire is surrounded by an insulating medium. Conversely, in any planar slice of the wire which is perpendicular to the gray plane (and still parallel to the z axis), there are no eddy currents because any math loop in such a plane sees no flux.

Non-uniform B_{ext}

Suppose now that the field $\mathbf{B}_{ext}$ has a positive linear gradient in the x direction. We can write,

$$j\omega\, B_{ext}(\mathbf{x},\omega) = j\omega[\, B_{ext0} + \alpha x] \qquad \Rightarrow \qquad \dot{B}_{ext}(\mathbf{x},t) = \dot{B}_{ext0} + \dot{\alpha}\, x \qquad \text{(P.5.4)}$$

Then,

$$\dot{B}_{ext}(\mathbf{x},t) = \dot{B}_{ext}(t) + \dot{\alpha}(t)\, x = j\omega\, e^{j\omega t}\, [\, B_{ext}(0) + \alpha(0)\, x\,] \ . \qquad \text{(P.5.5)}$$

We assume $\alpha(0) > 0$ so the B field magnitude is larger at the top of Fig P.8 than at the bottom at t = 0. Below we shall assume a time such that $e^{j\omega t} = -1$ so then both $\dot{B}_{ext}(t)$ and $\dot{\alpha}(t)$ are negative. Then the first equation of (P.5.3) becomes,

$$\partial_x J_z = \sigma \dot{B}_{ext} = \sigma\, [\dot{B}_{ext0} + \dot{\alpha}\, x\,] \qquad \Rightarrow \qquad J_z(x) = \sigma\, [\dot{B}_{ext0}\, x + (1/2)\, \dot{\alpha}\, x^2 - (1/6)\, \dot{\alpha}\,]$$

or

$$J_z(x) = -\sigma\, [\ |\, \dot{B}_{ext0}|\, x + (1/2)\, |\, \dot{\alpha}\, |\, x^2 - (1/6)\, |\, \dot{\alpha}\, |\ ] \qquad // \text{ for our time of interest} \qquad \text{(P.5.6)}$$

where we have added a constant such that $\int_{-1}^{1} dx\, J_z(x) = 0$ for a wire of radius a = 1. $J_{eddy} = J_z$ is now larger in the upper half of the gray rectangle than in the lower half, and we would expect then a pattern having this general shape,

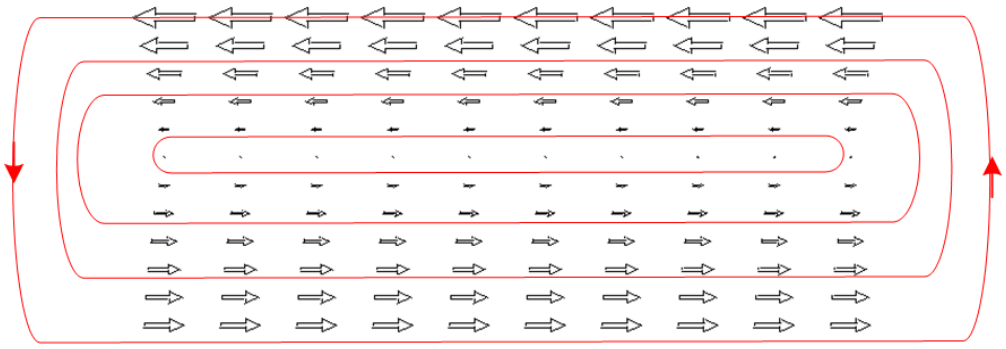

Fig P.10

The eddy currents are now larger on the side of the wire where the external field B_{ext} is larger. In addition, one sees the eddy current in general to be larger near the surface of the wire and small in the interior. Figure P.10 is analogous to Fig P.5 above which shows the eddy current in a thin round plate for a uniform external B field.

P.6 Eddy currents induced in an current-carrying wire by an external B field

We start with the self-induced eddy current pattern in a round wire shown in Fig P.7 (b),

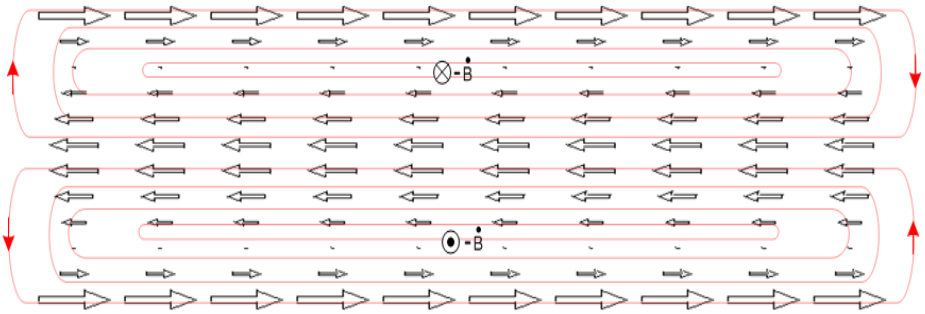

Fig P.7 (b)

We then turn on a uniform external B field which induces an additional eddy current pattern in the same round wire, as shown in Fig P.9,

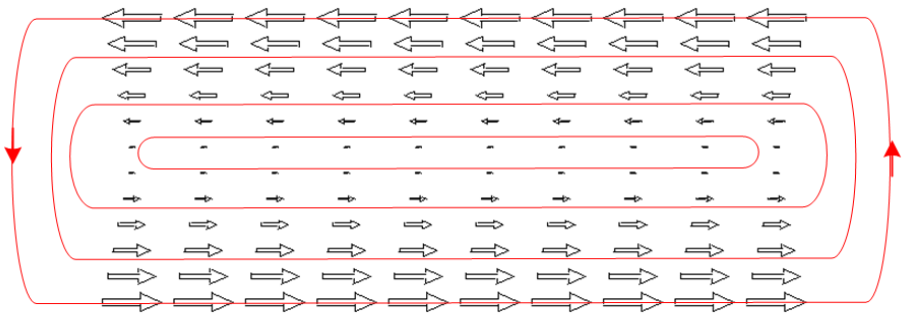

Fig P.9

We assume the external B field has the proper phase relative to the current in the wire such that the patterns look as shown above. When a small amount of the lower pattern is superposed on the upper

pattern, there is partial cancellation on the top edge, and reinforcement on the lower edge, resulting in the following eddy current pattern,

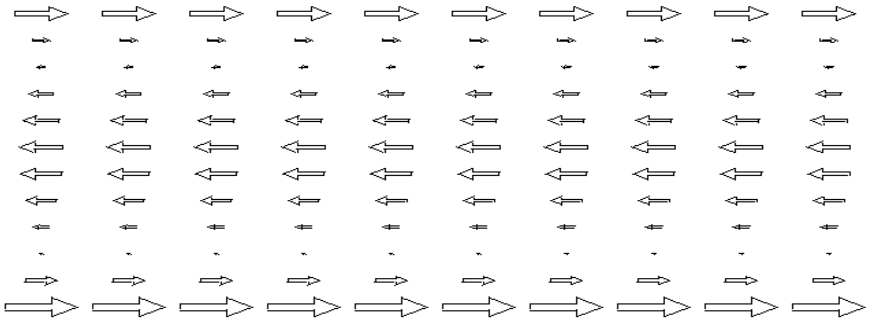

Fig P.11

Thus we arrive at another mechanism for the eddy current to be larger on one side of a wire than on the other side. Notice that B_{ext} has no gradient in this example, and also that we are not showing the underlying DC uniform current pattern of Fig P.7 (a).

P.7 Summary of Round Wire Examples

1. The eddy currents which a current-carrying round wire induces into itself vary with radius inside the wire, but are azimuthally symmetric. These eddy currents are interpreted as causing the skin effect. This situation is depicted in Fig P.7 (c).

2. A *quiet* round wire in the presence of a spatially-uniform external B field will have induced eddy currents which are oppositely directed on the two sides of the wire, but the absolute value of the current is symmetric on the two sides, as in Fig P.9.

3. If this *quiet* wire is placed in an external B_{ext} field which has a *gradient*, then the absolute value of the current density will be larger on the side of the wire where B_{ext} is larger, as shown in Fig P.10.

4. When a *current-carrying* round wire is placed in a uniform external B_{ext} field, even though that field is uniform, the absolute value of the current density is larger on one side of the wire compared to the other side, as shown in Fig P.11.

5 When a *current-carrying* round wire is placed in a external B_{ext} field which has a gradient, we again expect to have a side-to-side eddy current asymmetry which is a combination of the effects of items 3 and 4 above. The asymmetry will depend on the direction of the current in the wire and on the size and polarity of B_{ext}.

P.8 Eddy currents in Transmission Lines: The Proximity Effect

We consider a transmission line composed of two round wires and focus our attention on wire #1 as our Device Under Test. If wire #2 is far away, as in a wide-spaced twin-line, then B_{ext} created by wire #2 is roughly uniform at the location of wire #1, and we then have the current asymmetry of Case 4 above. If wire #2 is close to wire #1, then B_{ext} created by wire #2 will have a gradient over wire #1, and then we

have the asymmetry combination Case 5 above where both effects must be considered. In the following drawing, we show in cross section two round wires both of which carry current I in the same direction, out of the plane of paper.

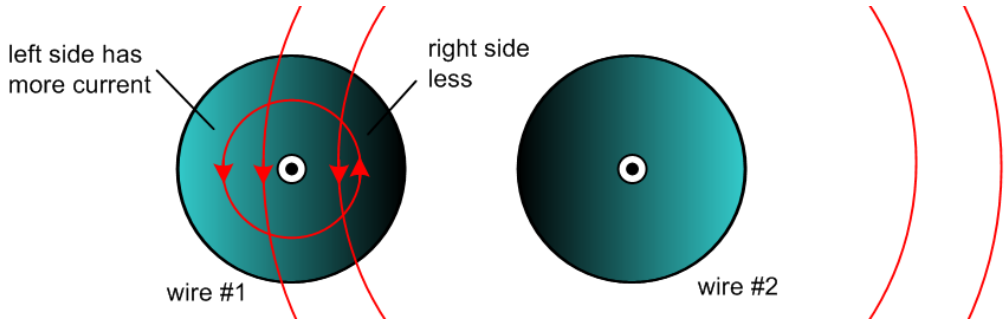

Fig P.12

The field B_{ext} created by wire #2 is slightly stronger on the right side of wire #1 than on the left side, which of itself would argue for more eddy current on the right side of wire #1. However this effect is swamped by the Case 4 effect where we have cancellation of B fields on the right side of wire #1 and addition on the left side, so the total B field is stronger on the left side of wire #1 and thus the eddy current (and hence the total current) is larger there, as indicated by the lighter coloration. The current asymmetry increases as the two conductors get closer together because both the B field cancellation and addition are enhanced as B_{ext} becomes larger and more comparable to the internal B field.

If we imagine positive charge carriers coming out of the plane of paper in wire #1, the ones on the left side of wire #1 feel a Lorentz force a q **v** x **B** pushing them to the right, while those on right side of wire #1 feel an oppositely directed force pushing them to the left. But the charge carriers on the right are in a smaller B field *and* travel at a smaller velocity v since $J_z = nqv$ is smaller. The net effect is that the charge carriers in wire #1 feel an overall force to the right and this force is transferred to the conductor ion lattice to maintain $\rho = 0$ causing the entire wire to be pushed to the right. The opposite happens inside wire #2 and the result is that wires with currents in the same direction attract each other.

The fact that the current distribution in each wire is skewed away from the other wire is sometimes called the **proximity effect**, or **current crowding**. One effect of having a non-uniform J_z distribution is that the wires have resistance larger than their DC values (see Section P.10 below). If the above two wires were two strands of a power transmission line cable carrying current in the same direction, the Ohmic loss in the strands is enhanced by this effect.

The coloration patterns in Fig P.12 don't really illustrate the skin effect which is of course always present at any $\omega > 0$, more strongly of course when $\delta < a$. Even in power lines at 60 Hz where $\delta \sim 1$ cm the skin effect does cause a waste of the wire interior since less current flows there. If a large round conductor is replaced by a set off smaller insulated round wires, this waste is reduced since the smaller wires each have more uniform current (see Litz wire).

In a normal transmission line the currents are of course oppositely directed and the picture is different:

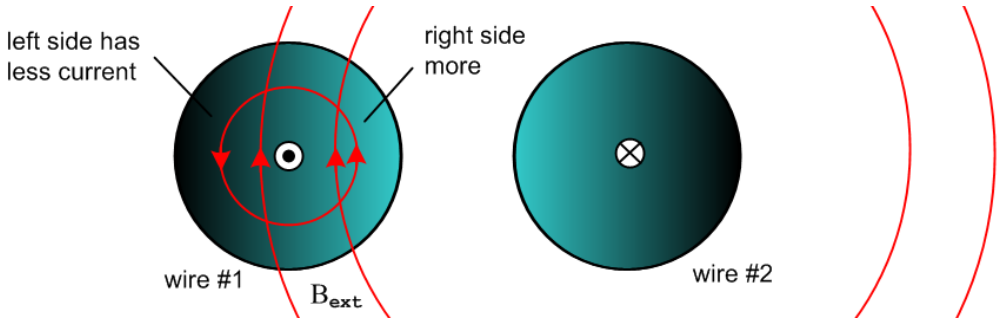

Fig P.13

Now the B field is larger on the right side of wire #1 so the eddy current is larger there causing the total current J_z to be larger there compared to the left side. The currents are now crowded on the side of each wire facing the other wire. The Lorentz force now causes the two wires to repel each other, reversing the argument given above. There is still Ohmic loss compared to DC since J_z is non-uniform. Closer wire spacing again results in increased asymmetry.

Companies like "Monster Cables" advocate using their low-ohm expensive cables for driving audio speakers in order to offset the resistance increases due to both proximity and skin effects.

Assuming a uniform J_z (zeroth order), it is not hard to compute the total magnetic field **B** of the two conductors at any point (x,y) in the cross-section plane. In the following graphs we show $|B_y(x,y=0)|$ (red) as a function of x in the y = 0 plane. The wires have radius 1/2 unit and center separation 3 units (the straight segments are not exactly straight) :

Currents in same direction:

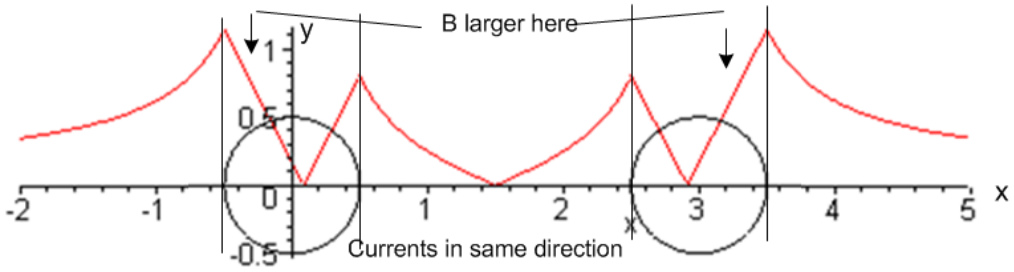

Fig P.14

Currents in opposite direction:

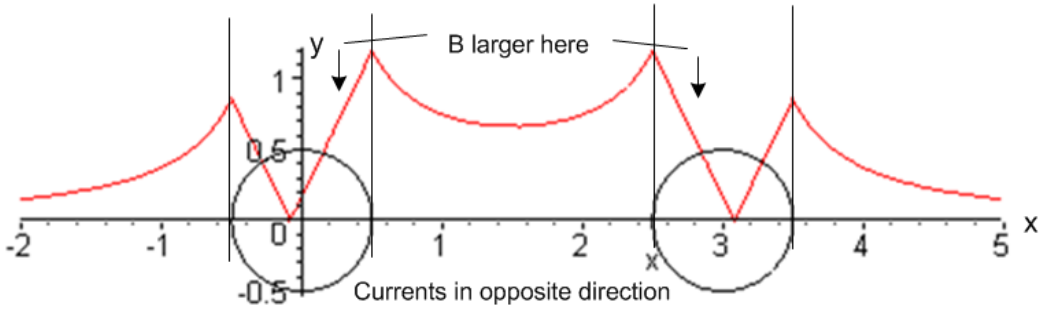

Fig P.15

These graphs support the claims made above about where the total B field is large and small, and thus where the eddy current is large and small. Of course the graphs are approximate since J_z is in fact not uniform on each wire cross section.

P.9 Quantitative Evaluation of Eddy Currents and The Proximity Effect

Our round-wire discussion above has all been qualitative, and no method was given for computing the actual size of the eddy currents and thus of the proximity effect for two parallel round wires. G. Smith presents the following intriguing chart showing the strength of the effect versus conductor separation under unspecified conditions,

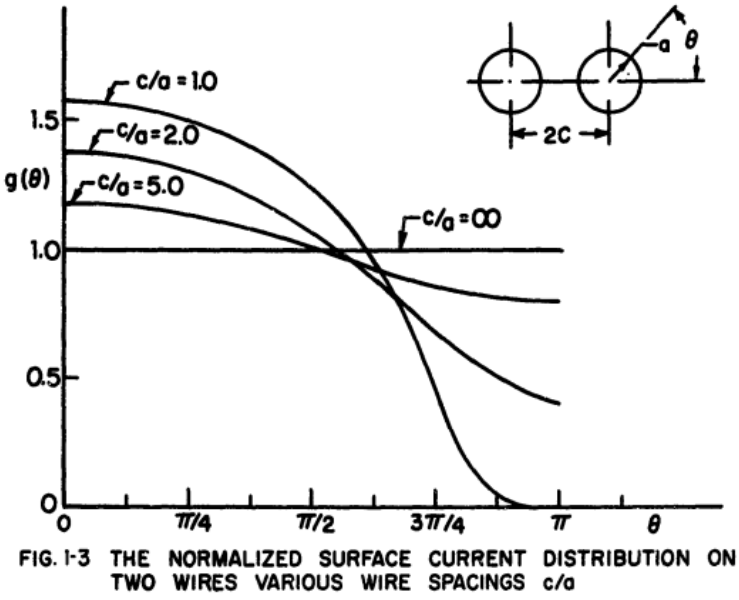

FIG. 1-3 THE NORMALIZED SURFACE CURRENT DISTRIBUTION ON TWO WIRES VARIOUS WIRE SPACINGS c/a

Fig P.16

Presumably ω is high enough to put the conductors into the skin effect regime so all currents are surface currents of thickness $\delta << a$.

We present in Chapter 7 a quantitative treatment of the skin and proximity effects for parallel round wires, and the results are similar to the above graph. Our treatment, however, is not based on eddy current analysis, but rather on the charge distribution on the conductor surfaces (think capacitance) and the radial charge pumping boundary condition (D.2.25) which causes internal currents to be larger where the time-changing surface charge is larger.

P.10 Influence of Proximity and Skin Effects on Wire Resistance

Consider a small differential volume $rd\theta drdz$ in a round wire (relative to a cylindrical coordinate system for that wire). Its cross sectional area is $dA = rd\theta dr$. This volume has resistance

$$dR = "\rho L/A" = \rho\, dz / dA \qquad (P.10.1)$$

and the current through this resistor will be

$$dI = J_z(r,\theta)\, dA \ . \qquad \text{(P.10.2)}$$

The Ohmic power generated in this tiny resistor is, from $P = I^2R$,

$$dP = (dI)^2(dR) = [J_z(r,\theta)dA]^2\, \rho\, dz / dA = \rho\, J_z(r,\theta)^2\, dA\, dz \ . \qquad \text{(P.10.3)}$$

For the coin-shaped resistor consisting of length dz of the entire round wire cross section we find then that

$$P = \int dP = dz \int dA\, \rho\, J_z(r,\theta)^2 \ . \qquad \text{(P.10.4)}$$

The total current in the wire is

$$I = \int dA\, J_z(r,\theta) \qquad \text{(P.10.5)}$$

and then from $P = I^2R$ the effective wire resistance of a cross sectional slice of wire of length dz is,

$$R = \frac{P}{I^2} = \rho dz\, \frac{\int dA\, [J_z(r,\theta)]^2}{[\int dA\, J_z(r,\theta)]^2} \qquad \int dA\, [...] = \int_0^a dr\, r \int_{-\pi}^{\pi} d\theta\, [...] \qquad \text{(P.10.6)}$$

Adding some cancelling factors of $A = \pi a^2$ we get,

$$\mathcal{R} = R/dz = [\rho/A]\, \frac{\int dA\, [J_z(r,\theta)]^2/A}{[\int dA\, J_z(r,\theta)/A]^2} = \mathcal{R}_{dc}\, \frac{\langle J_z^2\rangle}{\langle J_z\rangle^2} = \mathcal{R}_{dc}\, \frac{E(J_z^2)}{[E(J_z)]^2} \qquad \text{(P.10.7)}$$

where $\mathcal{R}_{dc}$ is the DC resistance per unit length of the wire. Our notations <> and E() mean "expected value". In elementary probability theory one writes

$\mu_x = E(X)$ // mean

$\sigma_x^2 \equiv var_x = E(X^2) - E(X)^2 = E(X^2) - \mu_x^2$ // variance; σ_x = standard deviation

so that

$$\frac{E(X^2)}{[E(X)]^2} = \frac{\sigma_x^2 + \mu_x^2}{\mu_x^2} = 1 + \frac{\sigma_x^2}{\mu_x^2} \ . \qquad \text{(P.10.8)}$$

Thus, taking $X = J_z$ we find this result for the round wire AC resistance per unit length,

$$\mathcal{R} = \mathcal{R}_{dc}\left(1 + \frac{\sigma_{Jz}^2}{\mu_{Jz}^2}\right) \qquad \frac{\mathcal{R}}{\mathcal{R}_{dc}} = 1 + \frac{\sigma_{Jz}^2}{\mu_{Jz}^2} \qquad \frac{P}{P_{dc}} = \left[1 + \frac{\sigma_{Jz}^2}{\mu_{Jz}^2}\right] \quad \text{// loss} \qquad \text{(P.10.9)}$$

At DC, J_z is constant across the wire cross section so its variance is 0 and the above says $\mathcal{R} = \mathcal{R}_{dc}$. For *any other* function $J_z(r,\theta) \neq$ constant, one will have some variance $\sigma_{Jz}^2 > 0$ and then $\mathcal{R} > \mathcal{R}_{dc}$. This discussion presented for a round wire of course applies to a wire of any constant cross sectional shape.

Thus, the proximity and skin effects increase the effective resistance of the wires in Fig P.12 or P.13, causing an increase in the Ohmic loss. Notice that the percentage proximity/skin-effect loss is independent of the current I.